Evaluation of Antennas in a Stepped Frequency Ground-Penetrating Radar for Location of Buried Objects

A. Snip, I.L. Morrow, P. van Genderen

Technical University of Delft, Faculty of Information Technology and Systems, International Research Centre for Telecommunications-transmission and Radar (IRCTR)

(Received October 15, 1998; accepted January, 1999.)

Abstract

In this paper we will present and discuss the design and material characterization of a small scale test environment. Then indicate some inherent limitations on such a small test site and outline one simple remedy to suppress near-field effects and environmental clutter.

Once the test environment is characterized a Stepped Frequency Ground Penetrating Radar is implemented using a Vector Network Analyser and used to critically investigate the performance advantages and limitations of a TEM horn and a standard gain horn used either in a monostatic mode or as part of a new bistatic configuration. This work demonstrated the standard gain horn in a bistatic configuration to be a more effective combination for detection of shallow and surface laid buried objects.

Keywords: Experimental, Stepped Frequency, Ground Penetrating Radar, Landmine Detection, RAM

INTRODUCTION

The detection of buried and surface laid objects using a variety of radar is currently receiving much attention. The use of pulse radar [1], frequency modulated continuous wave (FMCW) [2], synthetic aperture radar [3], and stepped frequency continuous wave (SFCW) radar [4] have all been reported. The experiments described here were all performed using a stepped frequency system.

In this section we describe the design and characterisation of the test environment and following that the SFCW GPR implementation and finally present our results for the GPR obtained using a number of antennas in different transmit/receive configurations.

To facilitate the testing of some GPR antennas using a stepped frequency radar system, it was advantageous to build a small scale indoor test environment. The IRCTR has available a number of large scale outdoor test and instrumentation sites for GPR work, however the merits of the small scale facility include:

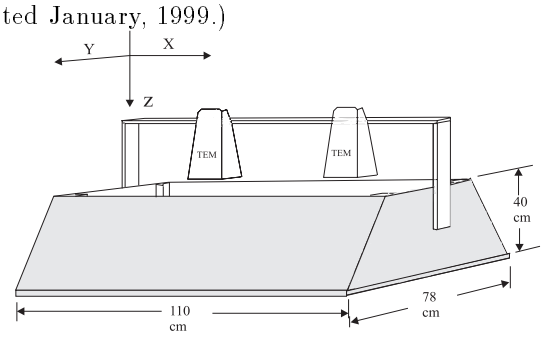

Figure 1: *Small test site. The antennas are manually moved in increments of 1cm or less to produce a single B-scan.*

- In-situ design and optimisation of antennas in the laboratory for work in the near field of material half space media.
- Experimental optimisation of transmit/receive antenna configurations prior to final outdoor testing.
- A test environment with very well defined material parameters, stable over long operating periods, thus aiding meaningful systems comparison.
- Reduced time and costs for outdoor testing.

Fig.1 shows a schematic of the indoor experimental setup. The box was constructed from plywood and filled with a local fine grain sand. The restrictions on the size of the box were primarily due to the high density of the sand (1600 kg/m^3) since this box was to be used indoors with a maximum allowable weight of 500 kg/m^2. The box has slanted side walls of 15^o to reduce specular reflections from the long sides (based on geometrical optics considerations). Due to the small size of the wooden box (1.1 m length x 0.75 m width x 0.4 m depth) it is particularity important to dampen internal EM reflections from the base of the box, since it is this background energy which sets the noise floor of any subsequent measurements. Thus, a low cost radar

absorbent material (RAM) was designed and optimised (across the 1.0-2.0 GHz frequency band) to be placed in contacted with the base of the box.

Design of an ultra-wide band GPR facility introduces new demands to the Radar Engineer; because of the broad spectrum of radio-frequencies involved, the common narrow band information on the electromagnetic properties of the constituent materials are inadequate. This is particularly true of absorbing materials who's frequency dependent properties can vary widely from DC to Gigahertz range. If real materials are to be used in the design and test of ultra-wideband systems, their properties must be known over the spectrum of interest.

Furthermore, such knowledge can be cast in the form of a compact representation (Debye etc.) suitable for computational electromagnetics (FDTD), to obtain realistic performance estimates from wideband radar systems [5].

Material measurement

Permittivity measurements were made in a rectangular waveguide sample cell over the frequency band from 1.12 to 1.7 GHz (WR650). The sample materials measured included the boxes construction material plywood (Delft), radar absorbent material (made in-house), and sand (granular size 100 μm, $\leq$ 10% moist. content). In the case of the sand the sample was contained by two Teflon (PTFE) containment windows 1.59 mm thick. The network analyser was calibrated using the TRL (Through, Reflect, Line) series of standards and a full 12 term error correction applied. For the sand measurements the PTFE windows were physically attached to the coaxial to waveguide transitions and their intrusion in the waveguide calibrated out. The measurement cell was then bolted between the transitions and the sample material inserted into the cell. Care must be taken to avoid air pockets in the sand sample, and in the case of the solid samples it is particularly important that the faces of the sample be flat after they have been placed in position. This minimizes the error associated with the reference plane positions.

The permittivity calculation are based upon the rather well known equations given in [6], here only the results obtained are presented. The technique assumes only a TE_{01} mode is propagating and that the guide is completely filled with a material of complex permittivity $\epsilon_r = \epsilon_r' - j\epsilon_r''$ where ϵ_r' is the dielectric constant and ϵ_r'' is the loss factor.

Material	Measured		Literature	
	$\overline{\epsilon_r'}$	$\overline{\epsilon_r''}$	ϵ_r'	ϵ_r''
Air	0.97	0.001	1.00	0.0
plywood (Delft)	2.10	0.35	2.1	-
RAM	1.50	0.23	-	-
sand (dry)	3.81	0.00	3-20	-

Table 1: *Comparison of measured ϵ_r for materials used in the test environment with values obtained from open literature [8]. Data is presented as an averaged value for the L-Band.*

To demonstrate the accuracy of the technique, trial measurements where made with an air sample. The measured value of air proved to be within 3% of its well known value, however the error associated with the other materials is larger 5-8%, due to the addition sources of error introduced in their measurement, for instance: sample homogeneity, uncertainty in references planes. Table 1 presents the measured frequency dependent permittivity as an *averaged* value over the frequency band for comparison with values obtain in the literature.

It can be seen that the measured values compare well with those obtained in the literature, but also provide additional useful information on the loss factor contribution for the plywood and RAM. It can be seen that the plywood has an unexpectedly high loss factor, thought to be due to the glue used in its manufacture process.

Optimisation of the RAM

The experimental setup was designed for antennas with an operating frequency band from approximately 1.0-2.0 GHz. The approach taken was to design and optimise a low cost RAM that could easily be manufactured and reconfigured for other bandwidths.

A multilayer structure was employed that consisted of alternate layers of dielectric and thin sheets of poorly conducting material [7]. The dielectric was chosen to be low-loss 9 mm double corrugated cardboard. The thin sheets of poorly conducting material were realized by depositing graphite on one side of the cardboard. Measurements in L-band waveguide determined the reflection coefficient of the structure for different numbers of layers. The absorber is of a resonant narrowband design

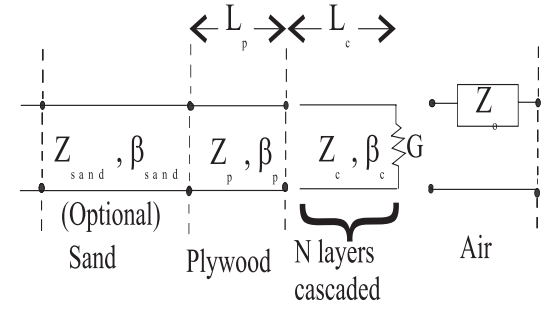

Figure 2: *Transmission line model*

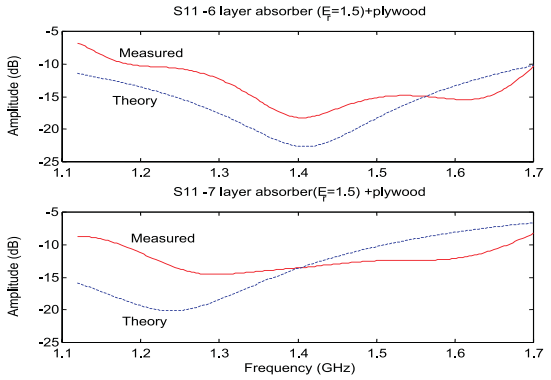

Figure 3: *Calculated and measured reflection coefficient for different numbers of sheets of absorber in contact with plywood*

and to help determine the number of sheets of RAM in contact with the plywood a theoretical transmission-line model was coded in MATLAB. The model is restricted to plane waves normal incidence and its transmission line representation is shown schematically in Fig.2.

Where $G = \overline{s}t$, $\overline{s} = 30k\Omega/$unit area is the average surface conductivity of the graphite layer, $t = 0.1$ mm the thickness of the sheet and $\epsilon_r' = 2.1$ the permittivity and $L_p = 18$ mm and length of plywood respectively.

All sections are assumed lossless. Each of the sections of transmission line are modelled as an ABCD matrix, these are then cascaded and the resultant two-port recovered and converted to equivalent S-parameters.

Fig.3 shows the measured and calculated results for the optimum number of layers for the frequency range of 1 to 2 GHz. The RAM theoretical narrow band performance compares well with commercial broadband RAM (AFP6 absorber has -23 dB @ 1 GHz), however its experimental values differ somewhat. This discrepancy may in part be due to the the RAM not making good contact with the waveguide walls or surface variation in the conductivity of individual sheets.

THE STEPPED FREQUENCY RADAR

A HP 8510B network analyzer is used as the coherent radar receiver. By sequentially measuring the phase difference between the transmitted and received signals at stepped operating frequencies the time delay to a buried object may be determined. The network analyser is connected to the antenna(s) mounted in the test environment (as shown Fig.1) via Sucoflex cable(s) and calibrated at the antenna terminals. Thus establishing a reference plane to which the returned signals phase will be rotated with respect to and adjusted for gain.

Depending on the configuration the associated S-parameters either in a monostatic S_{11}, or a bistatic S_{12} mode are recorded and sent to a PC via an HPIB interface for automated data collection and post-processing. The data collected at each physical measurement point consists of a reflection coefficient measurement or transmission measurement at N frequencies uniformly spaced over the frequency band.

The antenna(s) are then manually moved either singly or as a pair along the support boom in increments of $\Delta x \leq 1$ cm to produce a single B-scan image.

The returned signal from a complex scattering coefficient $s(z)$ at a distance z from the radar reference plane to the transmitted signal is given by,

$$S(f_n) = \frac{E_r(f_n)}{E_t(f_n)} = 1/z_0 \int_0^{z_0} s(z) exp(-2\pi f_n (\frac{2z}{v}))dz \quad (1)$$

were v is the velocity in the medium and the range resolution Δz possible with a SFCW radar using N steps of Δf is,

$$\Delta z = \frac{c}{2N\Delta f} \quad (2)$$

where $N\Delta f$ is the radar bandwidth. Range measured in this way is ambiguous after a maximum range of,

$$z_{max} = \Delta z N \quad (3)$$

setting $t = 2z/v$ and $n\omega_o = 2\pi f_n$ then the inverse Fourier transform is,

$$s(z) = \sum_{n=0}^{N-1} S(f_n) exp(j2\pi f_n(\frac{2z}{v})) \quad (4)$$

The complex Inverse Fast Fourier Transform (IFFT) is carried out on the corrected data producing a time domain (implied range) profile of reflected energy. An estimate of soil permittivity is required to convert this profile to exact range. At each frequency the signal may be integrated for as long as is convenient to scanning speed requirements. In this way the signal to noise is improved.

To counteract the influence of the near field radiation pattern of the antennas and local background reflections a simple remedy is applied. A B-scan of the background test environment without the presence of objects is first taken and then subtracted in post processing from the B-scan with objects buried as described in Eq.5.

$$s(z) = \text{IFFT}(S_{21}^{object}(x, f_n) - S_{21}^{empty}(x, f_n)) \quad (5)$$

RESULTS

The data for the performance of the SFCW system is now presented, using the experimental setup previously characterised and signal processing described earlier. The objective is to clearly discriminate mine-shaped metal and non-metallic objects buried in the sand.

Table 2 shows the buried position (w.r.t. Fig.1) of various objects in the sand-box. Amplitude and phase spectrograms, using a number of different antenna in various configurations are then generated for line scans of the box containing the objects. At each measurement point the transmission or reflection coefficient is measured at 401 different frequency points over two frequency bands ranging from 1.0-2.0 GHz or 4.0-6.0 GHz with an averaging factor of 32 at each frequency. The quantised distance into the sand $\epsilon_r = 3.81$ is 3.7 cm. The distance between the measurement points is 10 mm in the x-direction. The transmitting power for these measurements was 0.32 mW and no saturation of the receiver was observed. These measurements then formed the basis data of the signal processing using a 512 points IFFT.

The first antenna configuration examined used a TEM horn as transmitter and a receive antenna in our novel configuration in the 1-2 GHz frequency band. Radar images are obtained by combining the raw amplitude and phase data in an absolute magnitude plot as shown in Fig.4. This envelope profile of reflections versus time as recorded by the radar truely represents the resolution of the data by exploiting the similar changes in amplitude and phase seen in spectrograms but ignores the phase information concerning the reflection coefficient of buried objects returns. Reflections in time are converted to relative reflection coefficient in depth z along each physical scan line i.e. x position. The radar range $z = 0$ starts from the calibration plane at the antenna terminals and therefore also contains information on reflections within the antenna structure and air/ground interface. The range displayed in all the figures is relative in the sense that it is a function of the frequency band, antenna structure, number of points used in IFFT and the relative dielectric constant of the ground.

Position	$x(cm)$	$y(cm)$	$z(cm)$
plate 1	28	0.0	2.5
coke can	57	0.0	1.5
aluminium plate	28	0.0	8.0
aluminium sphere	52	0.0	6.0
plate 2	81	0.0	2.0

Table 2: *Centre co-ordinates of buried objects in ground (see Fig.1 for reference frame)*

The objects buried from left to right include dielectric plate 1 (ϵ_r=15), coke can and dielectric plate 2 (ϵ_r=5). To further enhance the definition of the scattered returns the post-processing background subtraction method mentioned in the previous section has been applied.

The three mine like objects are identifiable from the radar image. Most notably the object with low dielectric contrast is clearly discernible. It is noticeable there is an unusually strong contrast for this object, and this anomaly may be explained when the background image is viewed; there were strong local echos present, in this spatial region. This is an expected limitation of using such a small test environment but the implied inference that low dielectric contrast objects are nevertheless detectable is welcome.

Next a Scientific Atlantic standard gain horn (4.0-6.0 GHz) was substituted for the TEM horn and the same receive antenna used for receiver. The setup was similar to that used for the TEM horn. At the time

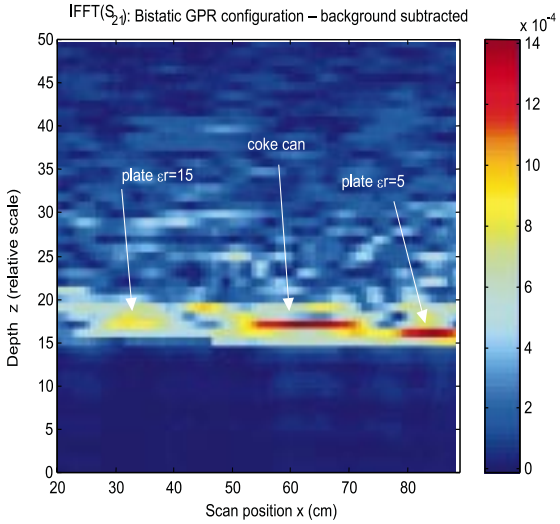

Figure 4: *Processed radar image from measured S_{21} data for TEM horn (Tx) and receive antenna (Rx). The intensities in the figure represent linear magnitude on a colour scale. Objects buried are: plate ϵ_r=15 depth=2.5 cm, coke can depth=2 cm, plate ϵ_r=5 depth=2.0 cm*

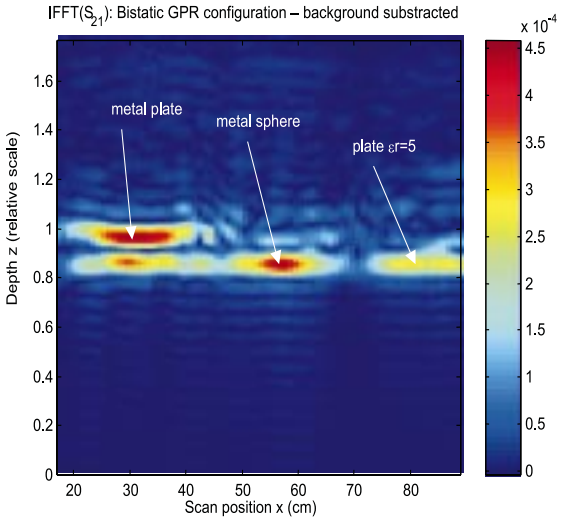

Figure 5: *Processed radar image from measured S_{21} data for standard gain horn (Tx) and receive antenna (Rx). The intensities in the figure represent linear magnitude on a colour scale. Objects buried are: aluminium plate (11.6 x 6.6 cms) depth=2.5 cm, aluminium sphere (diameter=6.0 cms) depth=6 cms, plate ϵ_r=5 depth=3.0 cm*

of writing it was not possible to make a direct comparison of antenna types in the same frequency band. The antenna configuration is the same as before to the air/ground interface. Fig.5 shows the measured results.

Even allowing for the resolution enhancement due to the step in frequency, the clarity of the image is very good and superior to the previous setup. All three objects are clearly visible with reflected energies commensurate with their material composition. The metal plate can clearly be seen to be buried deeper than the other object and has the strongest scattering. The secondary scattering seen above the main one is thought to be scattering from the air/ground interface.

The next GPR configuration investigated employed a monostatic configuration where only the reflection coefficient S_{11} of the antenna is recorded. The antenna is elevated 71.5 cms above the air/ground and E-plane vertically polarised. Fig.6 and Fig.7 show the results obtained for the standard gain horn and the TEM horn.

Comparing the results of the standard gain horn in monostatic mode with its bistatic configuration we see the advantage of our novel antenna configuration since its sensitivity limits its spatial extent within the broader footprint of the horn antenna. Clearly the results obtained (see Fig.7) using TEM horn indicate it is not, at

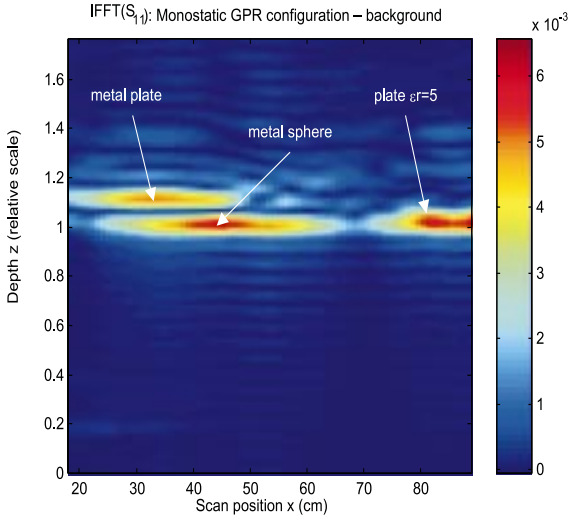

Figure 6: *Processed radar image from measured S_{11} data for standard gain horn (Tx/Rx). The intensities in the figure represent linear magnitude on a colour scale. Objects buried are: aluminium plate (11.6 x 6.6 cms) depth=8.0 cm, aluminium sphere (diameter=6.0 cms) depth=6 cms, plate ϵ_r=5 depth=3.0 cm*

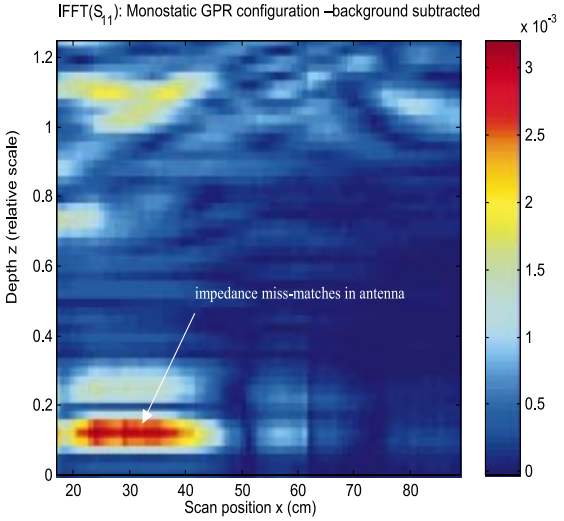

Figure 7: *Processed radar image from measured S_{11} data for TEM horn (Tx/Rx).The intensities in the figure represent linear magnitude on a colour scale. Objects buried are: aluminium plate (11.6 x 6.6 cms) depth=8.0 cm, aluminium sphere (diameter=6.0 cms) depth=6 cms, plate ϵ_r=5 depth=3.0 cm*

present, suitable for a monostatic configuration.

CONCLUSION

The design and material characterization of a small test environment for GPR work has been presented. It has been demonstrated that the test environment is suitable for low frequency and high frequency GPR antenna testing.

A stepped frequency radar system has been implemented using a Network Analyser and some signal processing theory outlined. A number of antennas types and antenna configurations have been investigated and thus-far the standard gain horn in a novel configuration with the receive antenna have demonstrated the best results. Miss-match losses and the open structure of the TEM horn, constrain its sensitivity and directional quality, and these are crucial parameters to the usefulness of the receive antenna. Further work is envisaged to design new antennas for near-field use and develop more sophisticated near-field clutter suppression techniques.

References

[1] L. C. Chan et al, A Characterisation of Subsurface Radar Targets, Proc. IEEE, vol.67, pp. 991-1000, 1979.

[2] K. Iizuka and P. Freundorfer, Detection of Non-metallic Buried Objects by a Stepped Frequency Radar, Proc. IEEE., vol. 71, pp. 276-279, Feb. 1983.

[3] Y. Nagashima et al, Single-unit Underground Radar utilizing Zero-crossed Synthetic Aperture, IEICE Trans. Commun, vol. E76-B, pp. 1290-1296, Oct. 1993.

[4] P.J. Clarricoats, Portable Radar for the Detection of Buried Objects, Radar 77 International Conference, IEE London, 1977.

[5] B. Sai, I.L. Morrow, P. van Genderen, Limits of Detection of Buried Landmines based on Local Echo Contrasts, EMC '98, October 1998.

[6] A.M. Nicholson and G.F. Ross, Measurement of the Intrinsic Properties of Materials by Time Domain Techniques, IEEE Trans. Instrum. Meas., vol. IM-17, pp. 395-402, Dec. 1968.

[7] C.G. Montgomery, R.H. Dicke, E.M. Purcell, Principles of Microwave Circuits, 1948, pp. 396-399.

[8] C. Balanis, Advanced Electromagnetic Engineering, Prentice Hall, 1989, pp.15.

Dr. I. L. Morrow, Technical University of Delft, Faculty of Information Technology and Systems, International Research Centre for Telecommunications Transmission and Radar (IRCTR) Mekelweg 4, 2628 CD Delft, Netherlands. E-mail: i.morrow@its.tudelft.nl, p.van genderen@its.tudelft.nl